amount of IgG in an ascites formation assay is dependent on the production rate of the hybridoma cells. Although these two assays reflect *in vivo* pathogenic activity of anti-Dsg3 IgG and subjective scaling can be used to represent the extent of the phenotypic results (Mahoney *et al.*, 1999; Aoki-Ota *et al.*, 2004), these assays do not measure pathogenic strength in a quantitative manner. To compare pathogenic strengths among pemphigus sera or anti-Dsg3 IgG mAbs, an *in vitro* dissociation assay was developed using primary cultures of human keratinocytes (Ishii *et al.*, 2005). In this study, we modified that assay using mouse keratinocytes to analyze the potential of each NAK mAb.

Under passive transfer, eight of 10 mAbs showed pathogenic activity and induced blister formation (Figure 3, Tables 1 and 2), while only two of eight AK mAbs, isolated from PV model mice receiving immunized $Dsg3^{-/-}$ splenocytes, were pathogenic (Tsunoda *et al.*, 2003). The higher frequency of pathogenicity among NAK mAbs is consistent with the fact that although mice receiving naive $Dsg3^{-/-}$ splenocytes showed lower titers of anti-Dsg3 IgG than did those receiving immunized splenocytes, the two types of mice showed no apparent differences in disease severity (Aoki-Ota *et al.*, 2004). The eight pathogenic NAK mAbs recognized Ca^{2+}-dependent epitopes on Dsg3, while the epitopes of the two nonpathogenic NAK mAbs were not dependent on Ca^{2+} (Table 1). Similar results have been seen with the AK mAbs: the two pathogenic antibodies were dependent on Ca^{2+}, while the six nonpathogenic AK mAbs were independent of Ca^{2+} (Tsunoda *et al.*, 2003). Most of pemphigus patients' IgG autoantibodies recognize Ca^{2+}-dependent epitopes on Dsg3 (Matis *et al.*, 1987; Eyre and Stanley, 1988; Amagai *et al.*, 1995). These findings together strongly suggest that pathogenic antibodies recognize Ca^{2+}-dependent conformational epitopes while nonpathogenic antibodies react with Ca^{2+}-independent linear epitopes.

Although eight of 10 NAK mAbs showed pathogenic activity in the passive transfer assay, none induced the PV phenotype in the ascites formation assay (Figure 4, Table 1), indicating that none were as potent as mAb AK23, which could induce the PV phenotype in adult mice upon hybridoma inoculation (Tsunoda *et al.*, 2003). More sensitive in vitro dissociation assays confirmed this and allowed us to rank the pathogenicity of NAK mAbs (Figure 5). In fine mapping using human Dsg1/Dsg3 point-mutated molecules, the epitopes of NAK 1 and 9, which crossreacted with human Dsg3, were mapped, respectively, to the amino-terminal T25, Y28, and Q29 and to T25, Y28, Q29, V53-N56 of Dsg3. These residues form a part of the adhesive interface of Dsg3 as predicted by crystal structure (Boggon *et al.*, 2002), but are different from the AK23 epitope (V3, K7, P8, and D59) (Tsunoda *et al.*, 2003). These findings suggest that the residues V3, K7, P8, and D59 may form the critically important part of the adhesive interface of Dsg3.

Although our attempt to isolate pathogenic anti-Dsg3 mAbs as potent as AK23 was not successful, pemphigus patients' sera always contain polyclonal anti-Dsg3 IgG autoantibodies, which recognize different parts of the molecule (Amagai *et al.*, 1992; Sekiguchi *et al.*, 2001). We therefore tested the possibility that a combination of several weakly pathogenic mAbs might show a synergistic effect and induce the PV phenotype in adult mice. Indeed, when the combination of hybridoma cells producing NAK1, 2, 4, and 7–11 were inoculated into $Rag2^{-/-}$ mice, the recipients developed the PV phenotype, with weight loss, patchy hair loss, and crusted erosions around the snout (Table 3). The minimal combination tested that was sufficient to induce the phenotype in all mice tested was NAK1, 2, 7, and 11 mAbs or NAK2, 3, 5, 11 mAbs (Figure 4). *In vitro* dissociation assays confirmed the synergistic pathogenic effects of NAK mAbs (Figure 5). This is the first demonstration of synergism among antidesmoglein IgG antibodies in inducing the loss of cell–cell adhesion of keratinocytes *in vivo* and *in vitro*.

In a previous study, AK mAbs recognizing the middle to C-terminal extracellular domain of Dsg3 did not show apparent pathogenic activity, suggesting that IgGs reacting with functionally less important parts of the molecule do not contribute to pathogenesis (Tsunoda *et al.*, 2003). However, in this study, NAK mAbs recognizing such regions showed synergistic effects with mAbs reacting with the N-terminal domain (e.g., mAbs NAK2, 3, and 9 or NAK2 and 11 in Figure 5c, Table 3). These findings provide molecular evidence that anti-desmoglein IgG antibodies recognizing the middle to C-terminal extracellular domains of Dsg3 can also take part in the pathogenic process of blister formation.

We knew that the dose of antibodies is an important factor to determine the pathogenic strength of patients' sera because antibody titers are generally correlated with the disease activities when monitored in individual patients (Sams and Jordon, 1971; Ishii *et al.*, 1997; Cheng *et al.*, 2002). We also knew that the epitope of antibodies is another important factor to determine the pathogenic strength of each anti-Dsg3 IgG (Tsunoda *et al.*, 2003). In this study, we demonstrated that the combination of different anti-Dsg3 IgG autoantibodies is the third important factor because most, if not all, patients' sera contain polyclonal anti-Dsg3 IgG. Thus, the clinical severity of the disease in each patient may be determined in a more complex manner than initially thought.

The preclinical condition in patients that precedes development of PV remains to be elucidated. One possibility is that one or a few nonpathogenic or weakly pathogenic anti-desmoglein IgG autoantibody (or autoantibodies) are first generated without inducing the apparent disease; additional autoantibodies recognizing different epitopes on desmoglein are subsequently produced, with the onset of the disease phenotype. It would be interesting to study whether signal transduction induced by the combined weakly pathogenic NAK mAbs and by the single AK23 mAb are different. Also of interest is whether long-term *in vivo* binding of weakly pathogenic antibodies induces any secondary inflammation in mice, including the recruitment of eosinophils. The weakly pathogenic anti-Dsg3 NAK mAbs together with the potent AK23 mAbs provide valuable tools to replicate and study the polyclonal condition as found in patients, and to dissect the molecular pathophysiology of pemphigus.

MATERIALS AND METHODS

Mice

$Dsg3^{-/-}$ offspring were obtained from matings of homozygotes (Amagai *et al.*, 2000b; Tsunoda *et al.*, 2002). These mice had the mixed genetic background of 129/SV ($H\text{-}2^b$) and C57BL/6J ($H\text{-}2^b$). Splenocytes (5×10^7) were prepared from naive $Dsg3^{-/-}$ mice, and adoptively transferred into C57BL/6 $Rag2^{-/-}$ mice (Central Institute for Experimental Animals, Tokyo, Japan) via the tail vein, as previously described (Aoki-Ota *et al.*, 2004). Anti-Dsg3 antibody production was examined by ELISA for recombinant mouse Dsg3, and *in vivo* binding against Dsg3 was confirmed by live keratinocyte staining (Tsunoda *et al.*, 2002). All mouse studies were approved by the Animal Ethics Review Board of Keio University.

Production of NAK mAbs

Splenocytes were isolated from mice that had the active PV phenotype and fused with P3 mouse myeloma cells at a ratio of 5:1 with PEG 4000 (Merck, Darmstadt, Germany), followed by selection with hypoxanthine–aminopterin–thymidine in the presence of 10% hybridoma cloning factor (IGEN, Gaithersburg, MD). Hybridoma cells were screened by ELISA using recombinant mouse Dsg3 and positive clones were further examined by live keratinocyte staining. Ten positive clones were screened and designated as NAK (AK mAb from PV model mice by naive splenocyte transfer) (Table 1). Each clone was obtained by three replicates of the limiting dilution method. The isotypes of mAbs produced were determined using an isotyping kit (Roche Diagnostics, Mannheim, Germany). Antibodies were purified from culture supernatants using the HiTrap rProtein A FF column (Amersham Biosciences, Buckinghamshire, UK).

ELISA and live keratinocyte staining

The reactivities of antibodies with mouse Dsg3, mouse Dsg1, human Dsg3, and human Dsg1 were measured by ELISA using the respective recombinant Dsg molecules, as described previously (Amagai *et al.*, 2000b; Tsunoda *et al.*, 2003; Anzai *et al.*, 2004). In brief, each sample was diluted 50,000-fold and run in duplicate. A standard serum obtained from a $Dsg3^{-/-}$ mouse immunized with $mDsg3^{-/-}$ was used as a positive control, and serum from a nonimmunized mouse was used as a negative control. The ELISA scores were calculated as index values using the formula: index value = (OD_{450} of sample − OD_{450} of negative control)/(OD_{450} of positive control − OD_{450} of negative control) × 100. Live keratinocyte staining was performed using the mouse keratinocyte cell line PAM212, as described previously (Amagai *et al.*, 2000b; Tsunoda *et al.*, 2003). To confirm calcium sensitivity of epitopes, an EDTA-treated ELISA was performed, incubating the ELISA plate with 5mM EDTA prior to the assay.

Epitope mapping by immunoprecipitation using chimeric desmogleins

Immunoprecipitation was performed using domain-swapped or point-mutated Dsg1/Dsg3 molecules to determine mAb epitopes (Tsunoda *et al.*, 2003; Anzai *et al.*, 2004). Typically, 3 μg of purified mAb and 200 μl of culture supernatant containing recombinant protein were mixed and incubated at room temperature for 30 minutes. These proteins were immunoprecipitated with protein G-Sepharose (Amersham Biosciences) overnight at 4°C. Anti-E-tag mAb (Amersham Biosciences) was used as a positive control. The immunoprecipitates were fractionated by SDS-PAGE and blotted onto a polyvinylidene difluoride membrane (Millipore, Bedford, MA). The recombinant proteins were visualized with an anti-6x histidine Ab (R&D Systems, Minneapolis, MN).

Passive transfer assays using neonatal mice

The pathogenic activities of the mAbs were evaluated by passive transfer in neonatal mice, an established assay for the pathogenic activity of pemphigus sera (Anhalt *et al.*, 1982; Amagai *et al.*, 1994). We injected NAK mAbs (120–250 μg/mouse, the highest dose we injected per mice) either alone or together with a small amount of total IgG prepared by ammonium sulfate precipitation of PF serum. The dosage of PF IgG was set at 50% of that needed to induce gross blistering, that is, 1 mg/mouse. Neonatal ICR (Institute of Cancer Research) mice (Sankyo Lab Service, Tokyo, Japan) were used at 12–24 hours after birth (body weight 1.5–2.0 g). The skin was evaluated grossly and microscopically 18–24 hours after injection. To evaluate microscopic blisters, the entire body skin was sectioned into six strips of about 3 mm in width. Blister formation was considered positive when the length of a single lesion was greater than 120 μm or when more than two acantholytic lesions were found after examining all six sections. Blisters found at the edges of sections were not counted. To quantify the extent of blister formation histologically, we calculated scores using the following formula: histologic blister score = ((combined total length of all blistered regions)/(combined total length of all sections examined)) × 100.

Ascites formation assay

To evaluate the pathogenic activity of the NAK mAbs in adult mice, we inoculated 5×10^6–1×10^7 cells, from individual hybridomas or from a mixture of clones, into the peritoneum of $Rag2^{-/-}$ mice primed with 2,6,10,14-tetramethyl-pentadecane (Wako Pure Chemical Industries, Osaka, Japan). The inoculated mice were monitored for ascites formation as well as for the appearance of the PV phenotype, manifested by weight loss and patchy hair loss. Biopsies of the oral mucous membranes and skin were taken when mice developed the PV phenotype or when ascites formation was observed after day 14.

In vitro dissociation assay

To evaluate the activity of mAbs in the inhibition of keratinocyte cell–cell adhesion, we modified a previously described *in vitro* dissociation assay (Ishii *et al.*, 2005). For this study, we used primary cultures of mouse keratinocytes rather than human keratinocytes. For these cultures, skin specimens prepared from neonatal ICR mice at 12–24 hours of age were incubated in dispase II (Roche Diagnostics Corp., Mannheim, Germany), and separated epidermis samples were further incubated in 0.25% Trypsin (Invitrogen, Carlsbad, CA). Isolated keratinocytes were dispensed into 12-well culture plates with keratinocyte culture medium CnT-02 (CellnTec, St Gallen, Switzerland). When keratinocytes were confluent, 1.2 mM calcium was added and cells were incubated for 24 hours. Recombinant exfoliative toxin A (0.25 μg/ml) produced in *E. coli*, which specifically digests mouse Dsg1 (Amagai *et al.*, 2000a; Amagai *et al.*, 2002), was added to cultures 2 hours before the assay, in which 1 μg/ml of individual or pooled NAK mAbs (1 μg/ml total) were added to culture media. After washing with 0.9 mM Ca^{2+}-phosphate-buffered saline

twice, mouse keratinocytes were incubated with dispase II for 15 minutes to release cells as sheets. Released sheets were carefully washed twice with 0.9 mM Ca^{2+}-phosphate-buffered saline and subjected to mechanical stress by pipetting with a 1 ml disposable pipette tip. Fragments were fixed by adding formaldehyde to a final concentration of 3% and were stained with crystal violet (Sigma-Aldrich Co., St Louis, MO). A cell sheet treated with 1 μg/ml of the positive control mAb AK23 was included in each assay to adjust for inter-assay variability. The mean number of particles was determined by counting with Image Pro software (Media Cybernetics Inc., Silver Spring, MD), using three sets of digital images captured for each plate. Dissociation scores were calculated from the number of fragments (*N*) as follows: Dissociation score = ((*N* with mAb − *N* without mAb)/(*N* with AK23 − *N* without mAb)) × 100.

CONFLICT OF INTEREST

The authors state no conflict of interest.

ACKNOWLEDGMENTS

We thank Dr Shoichiro Tsukita for the mouse myeloma P3 cells and for technical advice on the development of mAbs and Dr Takeji Nishikawa for critical discussion. We also thank Ms Yoshiko Fujii for the preparation of recombinant proteins, Ms Minae Suzuki for the immunofluorescence staining and Ms Hiromi Itoh for excellent animal care. This work was supported by Grants-in-Aid for Scientific Research from the Ministry of Education, Culture, Sports, Science and Technology of Japan; the Health and Labour Sciences Research Grants for Research on Measures for Intractable Diseases; the Ministry of Health, Labor and Welfare of Japan; and Keio Gijuku Academic Development Funds.

SUPPLEMENTARY MATERIAL

Figure 1. Immunostaining of mouse and human tissues with NAK mAbs that were not listed in Figure 1.

REFERENCES

Amagai M (1996) Pemphigus: autoimmunity to epidermal cell adhesion molecules. *Adv Dermatol* 11:319–52

Amagai M (1999) Autoimmunity against desmosomal cadherins in pemphigus. *J Dermatol Sci* 20:92–102

Amagai M (2003) Pemphigus. In: *Dermatology* (Bolognia J, Jorizzo J, Rapini R, Horn TD, Mascaro J, Mancini AJ, Salasche SJ, Saurat JH, Stingl G, eds), London: Harcourt Health Sciences, 449–62

Amagai M, Hashimoto T, Shimizu N, Nishikawa T (1994) Absorption of pathogenic autoantibodies by the extracellular domain of pemphigus vulgaris antigen (Dsg3) produced by baculovirus. *J Clin Invest* 94:59–67

Amagai M, Ishii K, Hashimoto T, Gamou S, Shimizu N, Nishikawa T (1995) Conformational epitopes of pemphigus antigens (Dsg1 and Dsg3) are calcium dependent and glycosylation independent. *J Invest Dermatol* 105:243–7

Amagai M, Karpati S, Prussick R, Klaus-Kovtun V, Stanley JR (1992) Autoantibodies against the amino-terminal cadherin-like binding domain of pemphigus vulgaris antigen are pathogenic. *J Clin Invest* 90:919–26

Amagai M, Klaus-Kovtun V, Stanley JR (1991) Autoantibodies against a novel epithelial cadherin in pemphigus vulgaris, a disease of cell adhesion. *Cell* 67:869–77

Amagai M, Koch PJ, Nishikawa T, Stanley JR (1996) Pemphigus vulgaris antigen (Desmoglein 3) is localized in the lower epidermis, the site of blister formation in patients. *J Invest Dermatol* 106:351–5

Amagai M, Matsuyoshi N, Wang ZH, Andl C, Stanley JR (2000a) Toxin in bullous impetigo and staphylococcal scalded skin syndrome targets desmoglein 1. *Nat Med* 6:1275–7

Amagai M, Nishikawa T, Nousari HC, Anhalt GJ, Hashimoto T (1998) Antibodies against desmoglein 3 (pemphigus vulgaris antigen) are present in sera from patients with paraneoplastic pemphigus and cause acantholysis *in vivo* in neonatal mice. *J Clin Invest* 102:775–82

Amagai M, Tsunoda K, Suzuki H, Nishifuji K, Koyasu S, Nishikawa T (2000b) Use of autoantigen knockout mice to develop an active autoimmune disease model of pemphigus. *J Clin Invest* 105:625–31

Amagai M, Yamaguchi T, Hanakawa Y, Nishifuji K, Sugai M, Stanley JR (2002) Staphylococcal exfoliative toxin B specifically cleaves desmoglein 1. *J Invest Dermatol* 118:845–50

Anhalt GJ, Labib RS, Voorhees JJ, Beals TF, Diaz LA (1982) Induction of pemphigus in neonatal mice by passive transfer of IgG from patients with the disease. *N Engl J Med* 306:1189–96

Anzai H, Fujii Y, Nishifuji K, Aoki-Ota M, Ota T, Amagai M *et al.* (2004) Conformational epitope mapping of antibodies against desmoglein 3 in experimental murine pemphigus vulgaris. *J Dermatol Sci* 35:133–42

Aoki-Ota M, Tsunoda K, Ota T, Iwasaki T, Koyasu S, Amagai M *et al.* (2004) A mouse model of pemphigus vulgaris by adoptive transfer of naive splenocytes from desmoglein 3 knockout mice. *Br J Dermatol* 151:346–54

Boggon TJ, Murray J, Chappuis-Flament S, Wong E, Gumbiner BM, Shapiro L (2002) C-cadherin ectodomain structure and implications for cell adhesion mechanisms. *Science* 296:1308–13

Cheng SW, Kobayashi M, Tanikawa A, Kinoshita-Kuroda K, Amagai M, Nishikawa T (2002) Monitoring disease activity in pemphigus with enzyme-linked immunosorbent assay using recombinant desmoglein 1 and 3. *Br J Dermatol* 147:261–5

Eyre RW, Stanley JR (1988) Identification of pemphigus vulgaris antigen extracted from normal human epidermis and comparison with pemphigus foliaceus antigen. *J Clin Invest* 81:807–12

Futei Y, Amagai M, Sekiguchi M, Nishifuji K, Fujii Y, Nishikawa T (2000) Conformational eptiope mapping of desmoglein 3 using domain-swapped molecules in pemphigus vulgaris. *J Invest Dermatol* 115:829–34

Ishii K, Amagai M, Hall RP, Hashimoto T, Takayanagi A, Gamou S *et al.* (1997) Characterization of autoantibodies in pemphigus using antigen-specific ELISAs with baculovirus expressed recombinant desmogleins. *J Immunol* 159:2010–7

Ishii K, Harada R, Matsuo I, Shirakata Y, Hashimoto K, Amagai M (2005) *In vitro* keratinocyte dissociation assay for evaluation of the pathogenicity of anti-desmoglein 3 IgG autoantibodies in pemphigus vulgaris. *J Invest Dermatol* 124:939–46

Koch PJ, Mahoney MG, Ishikawa H, Pulkkinen L, Uitto J, Shultz L *et al.* (1997) Targeted disruption of the pemphigus vulgaris antigen (desmoglein 3) gene in mice causes loss of keratinocyte cell adhesion with a phenotype similar to pemphigus vulgaris. *J Cell Biol* 137: 1091–102

Mahoney MG, Wang Z, Rothenberger KL, Koch PJ, Amagai M, Stanley JR (1999) Explanation for the clinical and microscopic localization of lesions in pemphigus foliaceus and vulgaris. *J Clin Invest* 103:461–8

Matis WL, Anhalt GJ, Diaz LA, Rivitti EA, Martins CR, Berger RS (1987) Calcium enhances the sensitivity of immunofluorescence for pemphigus antibodies. *J Invest Dermatol* 89:302–4

Sams WMJ, Jordon RE (1971) Correlation of pemphigoid and pemphigus antibody titres with activity of disease. *Br J Dermatol* 84:7–13

Sekiguchi M, Futei Y, Fujii Y, Iwasaki T, Nishikawa T, Amagai M (2001) Dominant autoimmune epitopes recognized by pemphigus antibodies map to the N-terminal adhesive region of desmogleins. *J Immunol* 167:5439–48

Shirakata Y, Amagai M, Hanakawa Y, Nishikawa T, Hashimoto K (1998) Lack of mucosal involvement in pemphigus foliaceus may be due to low expression of desmoglein 1. *J Invest Dermatol* 110:76–8

Tsunoda K, Ota T, Aoki M, Yamada T, Nagai T, Nakagawa T *et al.* (2003) Induction of pemphigus phenotype by a mouse monoclonal antibody against the amino-terminal adhesive interface of desmoglein 3. *J Immunol* 170:2170–8

Tsunoda K, Ota T, Suzuki H, Ohyama M, Nagai T, Nishikawa T *et al.* (2002) Pathogenic autoantibody production requires loss of tolerance against desmoglein 3 in both T and B cells in experimental pemphigus vulgaris. *Eur J Immunol* 32:627–33

Original Article

Cytogenet Genome Res 115:51–61 (2006)
DOI: 10.1159/000094801

Cytogenetic and Genome Research

Genomic structure of swine taste receptor family 1 member 3, *TAS1R3*, and its expression in tissues

S. Kiuchi[a] T. Yamada[b] N. Kiyokawa[c] T. Saito[a] J. Fujimoto[c] H. Yasue[a]

[a]National Institute of Agrobiological Sciences, Tsukuba, Ibaraki
[b]School of Medicine, Keio University, Shinjuku-ku
[c]National Research Institute for Child Health and Development, Setagaya-ku, Tokyo (Japan)

Manuscript received 18 October 2005; accepted in revised form for publication by H. Hameister, 9 February 2006.

Abstract. Taste receptor family 1 member 3, TAS1R3, is shown to be involved in sweet and umami tastes in mouse, and the nucleotide sequence of the gene has been reported in rat, gorilla, and human. Pigs are frequently used as models for human diseases, and are also considered to be source animals for xenotransplantation to humans due to their anatomical and physiological similarities to humans. Therefore, in the present study, the genomic structure of the swine *TAS1R3* gene was determined, and *TAS1R3* expression was studied in various swine tissues. The gene was shown to reside on swine chromosome 6q22→q23, from which three types of mRNAs were generated: 3,752 bp derived from six exons in tongue, 3,704 bp from six exons and 3,630 bp from seven exons in testis. The 6 exons/5 introns were structurally similar to those of humans and mice, but the 7 exons/6 introns structure of *TAS1R3* was first observed in swine. High expressions of *TAS1R3* were revealed in tongue, kidney, and testis by real-time PCR. The expression profile of the tissues except for kidney was similar to that of mouse. When in situ hybridization using an RNA probe for *TAS1R3* was performed on swine tongue and testis tissues, *TAS1R3* expressions were revealed in tongue circumvallate papillae, fungiform papillae, mucosal epithelium, follicular B lymphocytes, lymphocytes in submucosal tissues of lingual tonsil, and spermatogenic cells. Using peripheral mature B lymphocytes, the expression of *TAS1R3* in B lymphocytes was further confirmed by real-time PCR and sequencing of the real-time PCR product.

Taste consists of five modalities, that is, salty, sour, bitter, sweet, and umami. These modalities are necessary for growth and survival in animals. Physiological studies have indicated that taste receptor cells selectively respond to different tastants (Gilbertson et al., 1992; Bernhardt et al., 1996; Cummings et al., 1996). Electro-physiological studies have suggested that salty and sour tastants modulate taste receptor cell function by directly affecting specialized membrane channels (Kretz et al., 1999; Lin et al., 2004). On the other hand, taste responses to bitter, sweet, and umami are shown to be initiated by G-protein-coupled receptors (GPCRs) and transduced via G-protein signaling cascades (Gilbertson et al., 2000; Lindemann, 2001). Bitter tastants are detected by ~30 members of the taste receptor family 2 (TAS2R), a subfamily of the GPCRs. Most TAS2Rs are co-expressed in the same subset of taste receptor cells (Adler et al., 2000), suggesting that these cells function as generalized bitter detectors. Sweet and umami tastes are mediated by three members of the taste receptor family 1 (TAS1R), a distinct GPCR subfamily. TAS1Rs combine to assemble two heteromeric GPCR complexes. The complex of taste receptor family 1 member 2 (TAS1R2) and taste receptor family 1 member 3 (TAS1R3) serves as a sweet taste receptor (Nelson et al., 2001; Li et al., 2002; Zhao et al., 2003); and that of

Request reprints from Hiroshi Yasue
Genome Research Department
National Institute of Agrobiological Sciences, 2 Ikenodai
Tsukuba, Ibaraki 305-0901 (Japan)
telephone: +81-298-38-8664; fax: +81-298-38-8674
e-mail: hyasue@affrc.go.jp

1424–8581/06/1151–0051$23.50/0

Accessible online at:
www.karger.com/cgr

taste receptor family 1 member 1 (TAS1R1) and TAS1R3, as an umami taste receptor (Li et al., 2002; Nelson et al., 2002; Zhao et al., 2003). In the genetic analysis of mice strains showing differences in preference for sweet, it is suggested that the sequence polymorphisms causing amino-acid substitutions are associated with this preference (Max et al., 2001; Reed et al., 2004).

Recently, pigs have drawn the attention of many researchers not only as a model animal for human diseases but also as a resource for xenotransplantation to humans because of their anatomical and physiological similarities to humans (Tumbelson and Schook, 1996). In line with this and the fact that elucidation of the preferences in pig populations would help breeding in terms of feeding efficiency (one of the major factors in animal science), in the present study we have determined the genomic structure of swine *TAS1R3* and investigated the mode of *TAS1R3* gene expression in various tissues. The swine *TAS1R3* gene is similar to that of human and mouse with respect to its reported genome structure and expression. Furthermore, the present study for the first time has revealed an alternative splicing of *TAS1R3* in testis and *TAS1R3* expression in tongue mucosal epithelium, mature B lymphocytes, and spermatogenic cells. This may imply as yet unreported additional functions of TAS1R3.

Materials and methods

Pigs for preparation of tissues and cells

Three and a half month-old male pigs of Landrace or Landrace/Duroc/Largewhite composite were used to obtain tissue for both RNA and in situ gene expression analyses. The animals used in the present study received humane care as described in the Guidelines for the Care and Use of Experimental Animals (National Institute of Agrobiological Sciences Care Committee, Japan). Peripheral blood cells obtained from these pigs were applied to a cell-sorter (EPICS ALTRA; Beckman Coulter, CA, USA) using anti-CD21 antibody (VMRD, Inc., WA, USA) to obtain a mature B lymphocyte population. The process for the preparation of tissue samples followed the guidelines of animal ethics at the National Institute of Agrobiological Sciences. The pigs were euthanized by an intravenous injection of 10 ml of sodium pentobarbital. Immediately after respiration and heartbeat stopped, tissue samples were excised from tongue, heart, lung, stomach, intestine, liver, kidney, and testis to prepare RNA and to fix tissues in 4% (w/v) paraformaldehyde in phosphate-buffered saline.

Analysis of swine TAS1R3 gene structure

To obtain bacterial artificial chromosome (BAC) clones containing the *TAS1R3* gene, a swine genomic DNA BAC library constructed by Suzuki et al. (2000) was screened by PCR. Primers (forward: hT1R3-Ex2L, reverse: hT1R3-Ex2R in Table 1) for PCR were designed from the human sequence (GenBank/EMBL/DDBJ Data Bank Accession No. BK000152) showing a high similarity to the mouse *Tas1r3* sequence (Accession No. AF337039, AL670236.9). The fragment (200 bp) amplified from swine genomic DNA by PCR using the primers was sequenced to confirm that the sequence was orthologous to that of human *TAS1R3*. BAC clones were subsequently selected from the library, and the purified BAC-DNA was cleaved with *Hin*dIII, fractionated by electrophoresis, and hybridized with a digoxigenin-labeled swine DNA fragment amplified by the above primers (PCR DIG Probe Synthesis Kit: Roche Diagnostics, Mannheim, Germany). BAC-DNA fragments which hybridized to the digoxigenin-labeled fragment were subcloned into pBluescript KS(+) and sequenced using PRISM Ready Reaction BigDye Terminator Cycle Sequencing Kits (ver. 2) (Applied Biosystems, Calif., USA) and an ABI3100 DNA sequencer (Applied Biosystems).

Preparation of porcine RNA

RNA was prepared from 0.7–1.7 g tissue samples using the guanidinium thiocyanate acid-phenol-chloroform method with TRIzol reagent (Invitrogen, Calif., USA) and from the mature B lymphocytes using RNeasy (QIAGEN Sciences, Md., USA). The RNAs thus prepared were treated with DNase I (TAKARA, Shiga, Japan) at 37°C for 30 min, and then with phenol:chloroform. The amounts and purities of the resulting RNAs were estimated by their absorbance from 220 to 320 nm.

Analysis of TAS1R3 cDNA

First-strand cDNA was prepared from the RNA obtained by the above, following the procedure described by Suzuki and Sugano (2003), and then used to amplify the *TAS1R3*-specific DNA fragments by PCR using primer pairs (see Table 1) designed with a swine *TAS1R3* genomic sequence. Briefly, PCR was performed in a 50 μl reaction mixture containing 2 μl of the tongue or testis first-strand cDNA as a template, LA PCR buffer (without $MgCl_2$) (TAKARA), 1.5 mM $MgCl_2$, 400 μM dNTPs, 0.05 U/μl TaKaRa LA Taq (TAKARA) and 0.2 μM primer pair (forward: T1R3-ExStaF, reverse: T1R3-3R), as indicated in Table 1. PCR was carried out at 94°C for 1 min, followed by 40 cycles of PCR consisting of 30 s denaturation at 94°C, 30 s annealing at 60°C, and 4 min extension at 72°C, and finally an extension step at 72°C for 10 min. Secondary PCR was performed using an aliquot of the preceding PCR product and a nested pair of primers (forward: T1R3-ExStaF, reverse: T1R3-ExEndR) (Table 1). Amplified PCR fragments were cloned into pUC118 and sequenced by the primer-walking method.

In order to obtain the 5′ and 3′ terminal regions of the *TAS1R3* transcripts, 5′ and 3′ rapid-amplification-of-cDNA ends (RACE) analysis was performed with the 5′/3′ RACE kit (Roche Diagnostics), following the manufacturer's instructions. The primer pairs for the RACE analysis are described in Table 1. The DNA fragments obtained by the RACE analysis were cloned and sequenced as above.

Attempts to identify SNPs (single nucleotide polymorphisms) of TAS1R3 possibly related to tasting

The genomic DNAs of a swine from each of five breeds, viz, Göttingen, Largewhite, Duroc, Berkshire, and Japanese wild boar, two from Landrace, and two F_1 from a Meishan × Göttingen cross population (Mikawa et al., 1999) were sequenced to identify sequence polymorphisms for the sweet preference, as in mouse (Max et al., 2001; Reed et al., 2004).

Assignment of TAS1R3 to the IMpRH map

In order to assign *TAS1R3* to the IMpRH map (http://imprh.toulouse.inra.fr/), primer pairs were designed in the sequence of *TAS1R3* and examined to select those which amplified the expected sequences from swine genomic DNA but not from Chinese hamster genomic DNA. One of the primer pairs (forward: H6-2-R2, reverse: T1R3-Ex1R in Table 1) was used for typing of IMpRH panel DNAs which had been kindly provided by INRA (France) and the University of Minnesota (USA) for radiation hybrid (RH) mapping (Yerle et al., 1998). The typing procedure was the same as that described previously (Kiuchi et al., 2002). The typed data were submitted to the IMpRH server at http://imprh.toulouse.inra.fr/ (Milan et al., 2000) to obtain the likely position of *TAS1R3* on the IMpRH map.

Fluorescence in situ hybridization localization of TAS1R3 on swine chromosome

Swine peripheral blood cells (Landrace) were cultured and labeled with 5-BrdU as described previously (Awata et al., 1995). The cultured cells were treated with hypotonic solution and fixative, followed by spreading on glass slides as described previously (Yasue and Ishibashi, 1982). Chromosome spreads were then subjected to FISH as described previously (Awata et al., 1995) using probe DNA. For the probe DNA, BAC DNA (500 ng) containing the *TAS1R3* gene was labeled with biotin using a nick translation kit (Roche Diagnostics).

Table 1. Primer list

Project / Primer name	Primer positions[a] from / to	Sequence (5′–3′)	Size (mer)	Annealing temperature (°C)	PCR product size (bp)
BAC library screening /					
hT1R3-Ex2L (forward)		CTACGACCTCTTTGATACGTGCTC	24	61	200
hT1R3-Ex2R (reverse)		GCATGAGGAAGAAGCTGAAGAACT	24		
1st-PCR for cDNA cloning /					
T1R3-ExStaF (forward)	−37 / −16	TGCTCACTGCCATCCCTGCTGG	22	60	3,321
T1R3-3R (reverse)	+3828 / +3807	ACCCATGACTGGCTTGGTACTG	22		
2nd-PCR for cDNA cloning /					
T1R3-ExStaF (forward)	−37 / −16	TGCTCACTGCCATCCCTGCTGG	22	60	2,627
T1R3-ExEndR (reverse)	+3134 / +3113	GGCACCTTGACTACGTCTGAGG	22		
Synthesis of 1st-strand cDNA in 5′RACE /					
T1R3-Ex3R	+701 / +682	GAAGAAGGAGGGGAACGTCT	20		
1st-PCR in 5′RACE /					
Oligo dT-anchor primer (forward) (Roche)		GACCACGCGTATCGATGTCGACTTTTTTTTTTTTTTTV	39	57	
T1R3-Ex2R3 (reverse)	+541 / +522	AGCCGAAGAACTTGCCGGTG	20		
2nd-PCR in 5′RACE /					
PCR anchor primer (forward) (Roche)		GACCACGCGTATCGATGTCGAC	22	59	
T1R3-Ex1R (reverse)	+104 / +84	AGCACGTAGTGCCCTTGCATG	21		
1st-PCR in 3′RACE /					
T1R3-Ex67F (forward)	+2839 / +2859	CATGCTGGCCTACTTCATCAC	21	57	
PCR anchor primer (reverse) (Roche)		GACCACGCGTATCGATGTCGAC	22		
2nd-PCR in 3′RACE /					
T1R3-Ex67F2 (forward)	+2967 / +2986	ACCTGCCCAAGTGCTACCTG	20	59	
PCR anchor primer (reverse) (Roche)		GACCACGCGTATCGATGTCGAC	22		
RH mapping /					
H6-2-R2 (forward)	−203 / −182	GGTGGCATCAGAATAAGAGTCC	22	59	307
T1R3-Ex1R (reverse)	+104 / +84	AGCACGTAGTGCCCTTGCATG	21		
Real-time PCR for *TAS1R3* /					
tg-502T (TaqMan probe)		CCACCGTGTGTACCAGGTTCTCGTC	25		
tg-476F (forward)	+144 / +160	GCTGGGCGACAGGACAG	17	50	102
tg-577R (reverse)	+317 / +298	TTGATTTCCTCCACAGCCAT	20		
RNA synthesis from *EGFP* /					
T7p-EGFP-540F (forward)		AGTAATACGACTCACTATAGGGCGACCACTACCAGCAGAACA	42	59	218
dT18-EGFP-717R (reverse)		TTTTTTTTTTTTTTTTTTCTTGTACAGCTCGTCCATGC	38		
Real-time PCR for *EGFP* /					
FAM-EGFP-634T (TaqMan probe)		CCCAACGAGAAGCGCGATCACA	22		
U57608EGFP615F (forward)		GTCCGCCCTGAGCAAAGA	18	50	62
U57608EGFP676R (reverse)		TCACGAACTCCAGCAGGACC	20		
Synthesis of ISH Anti-Sense cRNA probe /					
T1R3-71F (forward)	+2854 / +2873	CATCACCTGGGTTTCCTTTG	20	57	165
T7-prm-T1R3-72R (reverse)	+2996 / +2977	AGTAATACGACTCACTATAGGGACCTCAGCAGCAGGTAGCAC	42		
Synthesis of ISH Sense cRNA probe /					
T7-prm-T1R3-71F (forward)	+2854 / +2873	AGTAATACGACTCACTATAGGGCATCACCTGGGTTTCCTTTG	42	57	165
T1R3-72R (reverse)	+2996 / +2977	ACCTCAGCAGCAGGTAGCAC	20		

[a] Positions based on the nucleotide number shown in Fig. 1.

Measurement of TAS1R3 gene expression by real-time PCR

An aliquot of each RNA sample was mixed with an amount of RNA fragment synthesized from pEGFP-C1 vector (EGFP: enhanced green fluorescent protein, Invitrogen), and the resulting mixture was subjected to synthesis of the first-strand cDNA using SuperScript III (Invitrogen), 5 μM Random Hexamer and 500 μM dNTPs, following the manufacturer's procedure. The RNA fragment from EGFP was prepared using a primer pair (forward: T7p-EGFP-540F, reverse: dT18-EGFP-717R in Table 1) with the AmpliScribe T7 High Yield Transcription Kit (EPICENTRE, Wisc., USA), and was then used as a monitor for reverse transcription efficiency and a standard for a quantitative comparison of *TAS1R3* transcripts among the samples. Samples subjected to synthesis of the first-strand cDNA were treated with RNaseH (TOYOBO, Osaka, Japan) at 37°C for 20 min. First-strand cDNA derived from *TAS1R3* transcripts in the samples was detected using TaqMan Universal Master Mix (Applied Biosystems), TaqMan probe (tg-502T) and the primer pair (forward: tg-467F, reverse: tg-557R), according to the procedure recommended by Applied Biosystems (ABI 7700). The first-strand cDNA derived from EGFP RNA was detected using TaqMan Universal Master Mix (Applied Biosystems), TaqMan probe (FAM-EGFP-634T) and a primer pair (forward: U57608EGFP615F, reverse: U57608EGFP676R). Primer sequences are listed in Table 1.

Prior to measurement, the fragment amplified from the tongue sample with the primer pair for *TAS1R3* was sequenced to confirm that

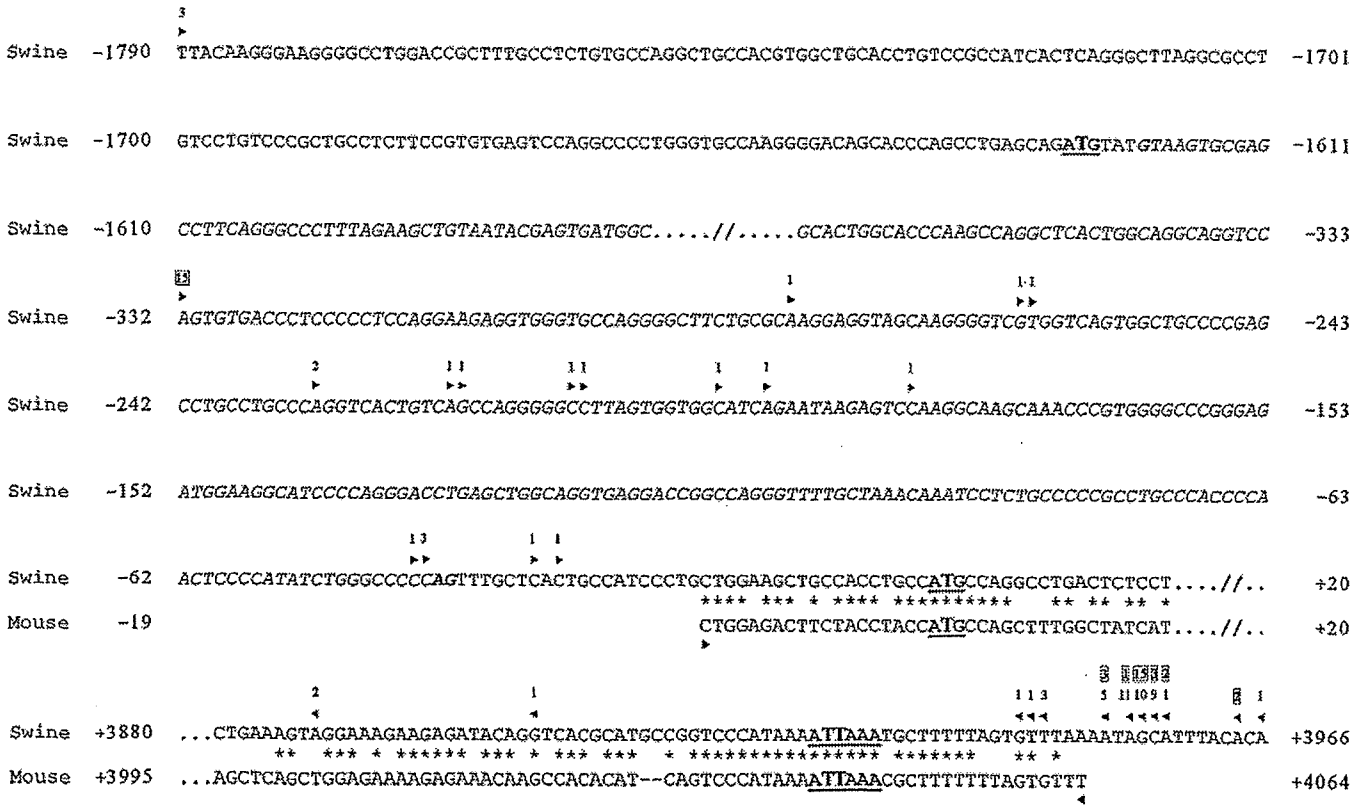

Fig. 1. Transcription initiation and termination sites of swine *TAS1R3*. The *TAS1R3* genomic sequence was numbered downstream of the transcription with the putative translation start site of Tonguel as +1. That start site and polyadenylation signal site are denoted by bold letters and underlines. The sequence indicated to be the intron for Tes2 transcription is shown in italics. Downstream arrowheads with boxed and unboxed numerals indicate initiation sites of the transcription in tongue and testis, respectively. Upstream arrowheads with boxed and unboxed numerals indicate termination sites of the transcription in tongue and testis, respectively. The numerals represent the number of clones showing initiation or termination of the transcription at the site of each arrowhead in the RACE analysis. As a reference, part of the mouse sequence was aligned with a swine sequence to show the transcription initiation and termination sites reported in mouse (Accession No. AF337039 and AL670236.9).

the primer pair amplified the expected sequence. In addition, it was confirmed that the DNA fragment from EGFP RNA was proportionally amplified depending on the amount of EGFP RNA used for real-time PCR.

Detection of gene expression site in tissues by in situ hybridization

After dissected tissues were fixed overnight in paraformaldehyde solution, they were embedded in paraffin and then sectioned 4 μm thick. Sections were collected on glass-slides and subjected to in situ hybridization. The procedure for in situ hybridization was the same as that reported earlier (Ohtsuki et al., 1998) with the following exception: hybridization was performed in a solution containing 50% formamide, 2× SSC, 1.0 mg/ml tRNA, 1.0 mg/ml salmon sperm DNA, 1.0 mg/ml BSA, 10% dextran sulfate, 1.0% SDS, and 8.0 μg/ml RNA anti-sense or sense probe at 37°C for 16 h. Hybridization signals were detected with the NBT/BCIP system (Sigma-Aldrich, Mo., USA).

For the RNA probe, DNA fragments were first prepared by PCR from *TAS1R3* cDNA using primer pairs T1R3-71F:T7-prm-T1R3-72R, and T7-prm-T1R3-71F:T1R3-72R. The sequences of primers are listed in Table 1. Using the DNA fragment obtained with the primer pair T1R3-71F:T7-prm-T1R3-72R and using the AmpliScribe T7-Flash Transcription Kit (EPICENTRE), a digoxigenin-labeled RNA anti-sense probe was prepared according to the manufacturer's instructions. With the same procedure, a digoxigenin-labeled RNA sense probe was prepared using the DNA fragment obtained with the primer pair T7-prm-T1R3-71F:T1R3-72R.

Results

TAS1R3 gene

A swine genomic DNA BAC library was screened to obtain three BAC clones containing at least a part of the putative *TAS1R3* gene. DNA from the BAC clones was processed as described in Material and methods to identify a *Hin*dIII fragment (about 6.6 kb) that contained the putative *TAS1R3* gene. The 6.6 kb fragment of one BAC clone (code 994D12) was cloned in pBluescript KS(+) and sequenced. In addition, cDNA fragments (2,627 bp) of *TAS1R3* transcripts from tongue tissue were generated using the primer pairs listed in Table 1, cloned into pUC118 vector, and sequenced. Since 5′/3′ regions of the putative *TAS1R3* gene transcript were likely to be missing from the cDNA sequences, RACE analysis was performed using the RNA prepared from tongue to determine the sequences of the 5′/3′ terminal regions. Fifteen fragments obtained by 5′ RACE were sequenced, revealing that all the transcriptions initiated from nucleotide position −332 (numbered from the translation start nucleotide in the 3′-direction in the present study). The sequenc-

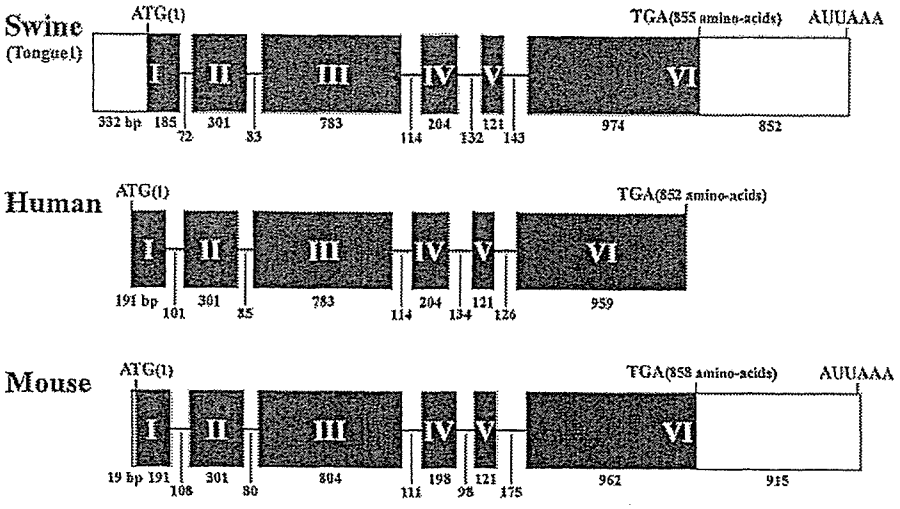

Fig. 2. Schematic presentation of swine *TAS1R3* gene structure. Boxes denote exons, with white parts representing 5′-untranslated region (UTR) and 3′UTR; and black parts signifying protein-coding regions. Exons are numbered according to their correspondence with those of human and mouse. As a reference, the genomic structures of human and mouse *TAS1R3* genes are included in this figure. The accession numbers for human and mouse cDNA of *TAS1R3* genes are BK000152 and AF337039, respectively. Those for human and mouse genomic DNA are NT_077965.1 and AL670236.9, respectively.

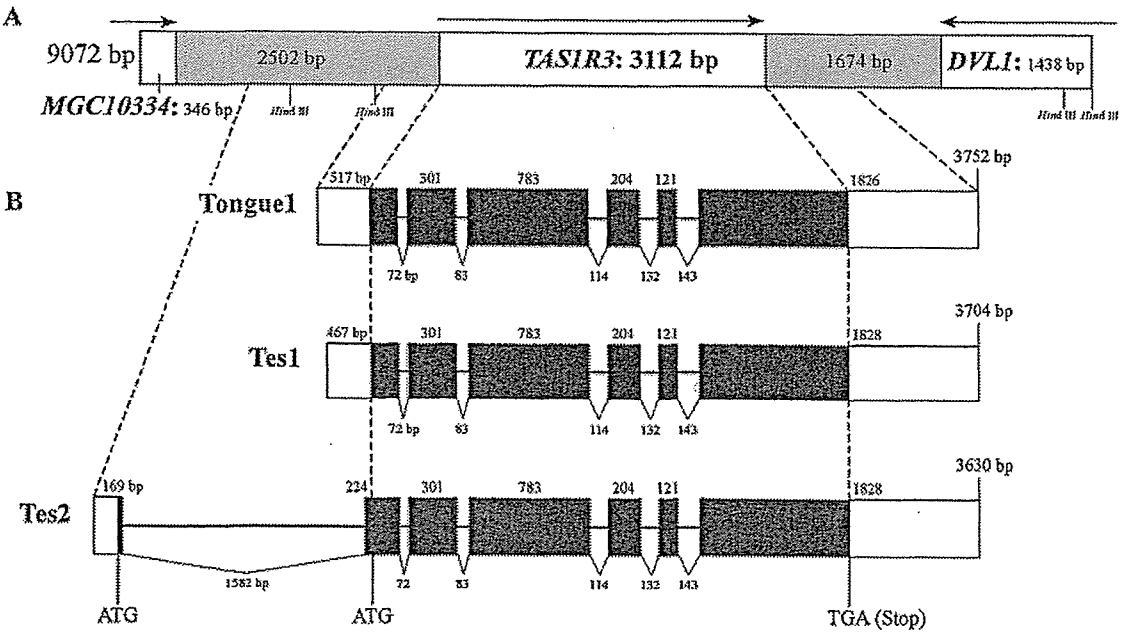

Fig. 3. Correspondence of swine *TAS1R3* transcripts to genomic sequence. (**A**) Swine genomic structure of the region encompassing *TAS1R3*. Regions tagged with *MGC10334* and *DVL1* correspond to human *MGC10334* and *DVL1*, respectively, based on sequence similarities. (**B**) Swine *TAS1R3* genomic structures, from which *TAS1R3* transcripts, Tongue1, Tes1, and Tes2, were derived. The reconstituted longest transcript in each type is presented in this figure. Symbols and markings in this figure are the same as those in Fig. 2.

ing of 26 fragments in 3′ RACE demonstrated that the transcriptions terminated at the nucleotide positions ranging from +3953 to +3964 (Fig. 1).

The reconstituted longest cDNA sequence (3,752 bp; from −332 to +3964 of the swine genomic sequence) (Tongue1: Accession No. AB162127) was then compared with the swine genomic sequence determined in the present study, revealing that swine putative *TAS1R3* consists of six exons and five introns, spanning 4,296 bp (Accession No. AB162126) (Fig. 2). When the structure of the putative *TAS1R3* gene was compared with those of human and mouse *TAS1R3* genes, it was found that their genomic structures were the same, though slight differences in the lengths of exons and introns were observed (Fig. 2). When the protein-coding sequence of Tongue1 was compared with that of human and mouse, the similarities between swine and human, and between swine and mouse were found to be 81.1% and 73.9%, respectively. These findings taken together led us to

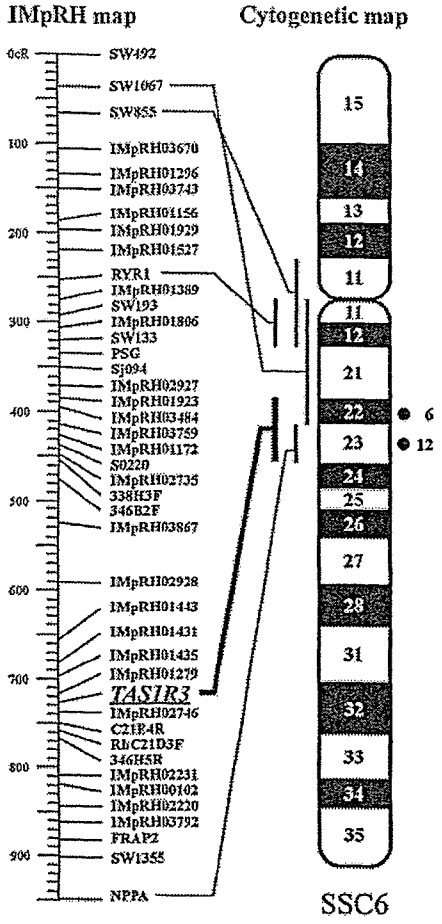

Fig. 4. Chromosomal location of swine *TAS1R3*. The position of *TAS1R3* (shown with italic and underline) on the IMpRH map was indicated. *TAS1R3* was assigned to the map by the RH mapping procedure described in Materials and methods (http://imprh.toulouse.inra.fr/). In addition, the chromosomal position of *TAS1R3* was determined by FISH, also described in Materials and methods. Hybridization signals obtained in FISH were scored along bands of the SSC6 ideogram, and presented as closed circles with the number of signals scored.

conclude that this swine putative *TAS1R3* gene is the orthologue of human and mouse *TAS1R3* genes.

Max et al. (2001) observed that *TAS1R3* mRNA of mouse testis showed a size difference from that of mouse tongue. Therefore, swine *TAS1R3* mRNA derived from testis was examined as in the case of tongue mRNA. This analysis revealed that two types of mRNA were generated from the *TAS1R3* gene in testis: one (Tes1: Accession No. AB162128) was the same as the tongue type, except that its transcription initiation sites varied in range from −282 to −31; the other (Tes2: Accession No. AB162129) contained an additional 45-bp protein-coding sequence upstream from the translation start site observed in Tongue1 and Tes1, which provided an additional 15 amino-acids to the deduced TAS1R3 protein encoded by Tongue1 and Tes1. The transcription termination sites of Tes2 were found to be similar to those of Tongue1 and Tes1. In order to determine the genomic structure for Tes2 production, the BAC-DNA was additionally sequenced, and compared with Tes2 sequences. It was revealed that Tes2 was derived from seven exons, which is the result of alternative splicing of *TAS1R3* as shown in Fig. 3.

Chromosomal assignment of TAS1R3

The swine genomic sequence containing *TAS1R3* (Accession No. AB162126) was compared with the corresponding human and mouse sequences. That comparison demonstrated that the arrangement of genes, i.e., *MGC10334-TAS1R3-DVL1* in swine (Fig. 3A), was the same as that of human and mouse, showing that the genomic region encompassing *TAS1R3* has been conserved at least in those three species. RH mapping was performed to assign the gene to the IMpRH map of swine chromosome (SSC) 6 between IMpRH01279 and IMpRH02746 (Fig. 4). We also carried out FISH to locate the gene physically on SSC6. FISH, as shown in Fig. 4, demonstrated that *TAS1R3* resides on SSC6q22→q23; this result is consistent with that of RH mapping.

Amino-acid sequence of TAS1R3

The amino-acid sequences derived from Tongue1 (or Tes1) and Tes2 were aligned with human and mouse TAS1R3 (Fig. 5). Based on the annotation of human and mouse TAS1R3, a signal peptide (http://www.cbs.dtu.dk/services/SignalP/), an ANF-receptor domain (receptor family ligand binding region), and a 7tm_3 domain (metabotropic glutamate family) (http://www.ncbi.nlm.nih.gov/BLAST/) were identified in the swine TAS1R3 amino-acid sequence of the alignment (Fig. 5).

When swine TAS1R3 derived from Tongue1 (or Tes1) was compared with that of human and mouse, the overall similarities of TAS1R3s between swine and human and between swine and mouse were calculated to be 75.1% and 71.6%, respectively. The similarities between swine and human, and between swine and mouse for the signal peptide region were calculated to be 47.1% and 50.0%, respectively, while those for the ANF-receptor domain were 74.5% and 72.6%, and those for the 7tm_3 domain were 81.7% and 76.6%, respectively. The borders between exons for swine, human, and mouse all occurred at the same positions in the alignment shown in Fig. 5, which is additional evidence for the similarity of the *TAS1R3* gene among the three species.

Since an additional 15 amino-acids were observed at the N-terminus of the protein derived from Tes2 compared to that from Tongue1 (or Tes1), the deduced amino-acid sequence from Tes2 was subjected to a web analysis for signal

Fig. 5. Alignment of swine, human and mouse TAS1R3 amino-acid sequences. The protein deduced from Tongue1/Tes1 comprises 855 amino-acids, and that from Tes2 870 amino-acids. Amino-acid sequences of proteins were aligned with human and mouse TAS1R3 using Genetyx (Software Development Co., Ltd., Tokyo, Japan). The amino-acids of Tes2 identical to those of Tongue1/Tes1 are shown by dots.

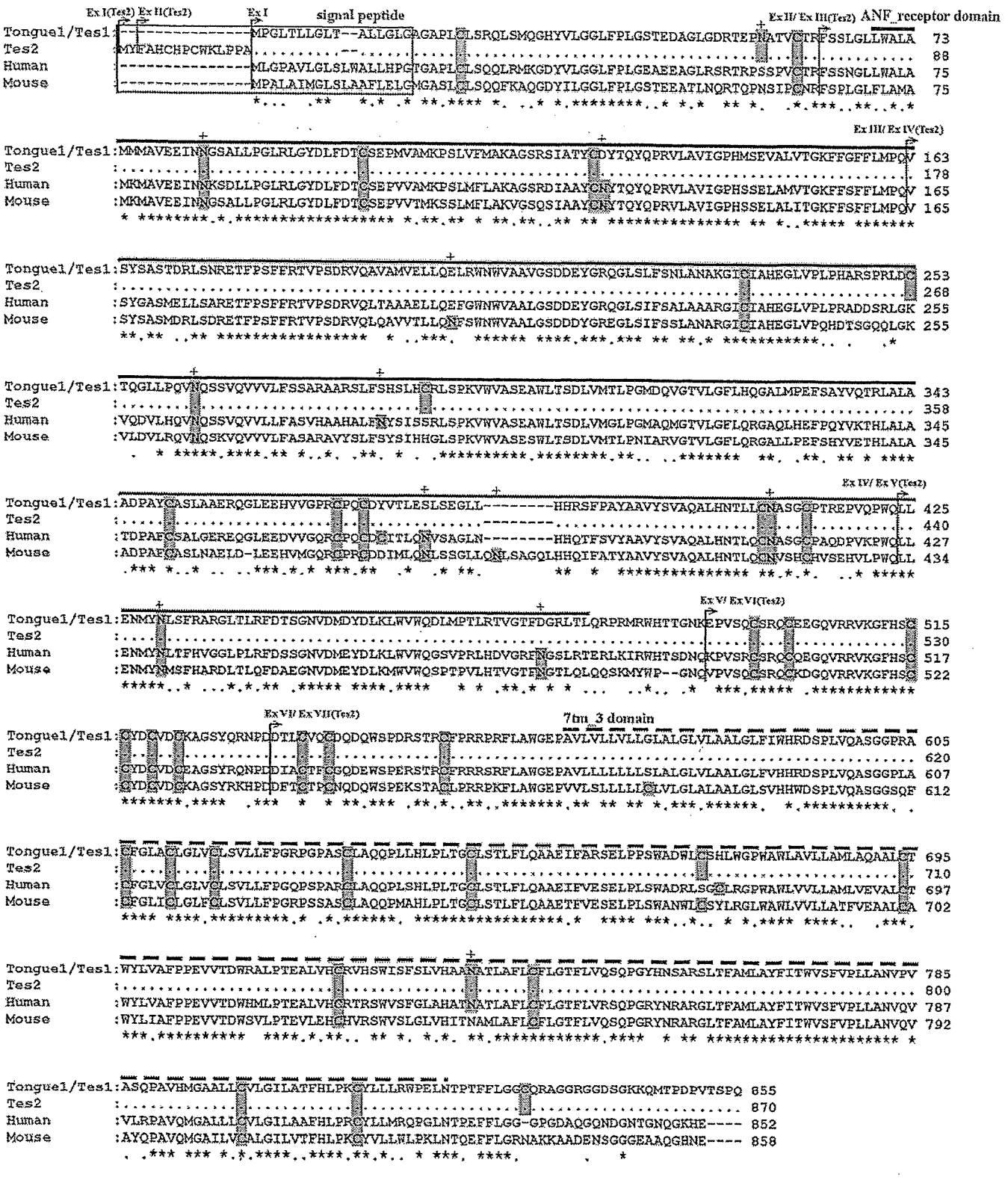

Putative signal peptide (http://www.cbs.dtu.dk/services/SignalP/) is boxed. The putative ANF-receptor domain (http://www.ncbi.nlm.nih.gov/Structure/cdd/cddsrv.cgi?uid=pfam01094&version=v2.04) and putative seven transmembrane domain (7tm_3 domain; http://www.ncbi.nlm.nih.gov/Structure/cdd/cddsrv.cgi?uid=pfam00003&version=v2.04) are marked by the solid and broken lines over the sequence, respectively. Potent N-linked glycosylation sites and cysteine residues are indicated by gray boxes with and without '+', respectively. Amino-acids conserved among swine, human, and mouse in the alignment are indicated by asterisks. Four out of six potent N-linked glycosylation sites and 29 out of 33 cysteine residues in swine are conserved in the three species.

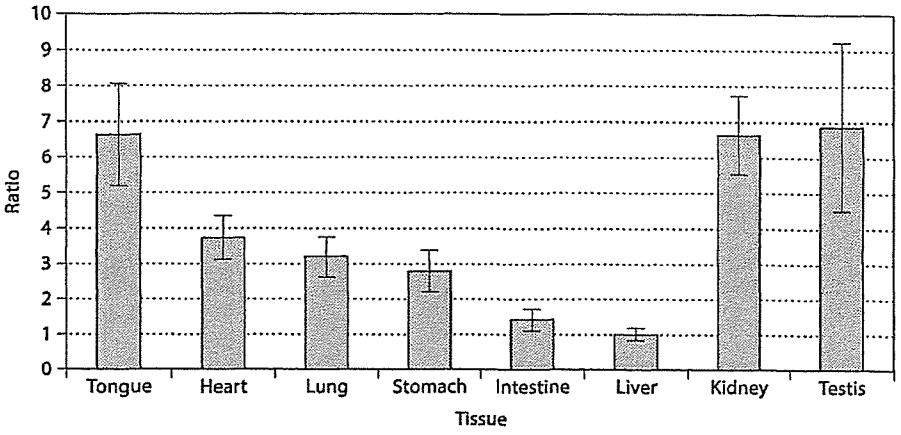

Fig. 6. Measurement of *TAS1R3* gene expressions in tissues by real-time PCR. RNA was prepared from tongue, heart, lung, stomach, intestine, liver, kidney, and testis, and subjected to real-time PCR as described in Materials and methods. Eight real-time measurements were made for each tissue sample, and mean values and standard errors were calculated for each sample. Values thus obtained were recalculated taking the mean value of liver as 1.0, and resulting values were plotted in this figure.

peptide (http://www.cbs.dtu.dk/services/SignalP/). The entire region of 33 consecutive amino-acids (i.e., 15 amino-acids plus the 18 amino-acid sequence corresponding to the signal peptide of the protein from Tonguel) at N-terminus of the protein from Tes2, was recognized as signal peptide. Therefore it is likely that TAS1R3 generated from Tes2 is functionally identical to those from the other transcripts.

DNA sequences of possible control region for TAS1R3

Since the 346 bp at the 5′ terminus of the 2,848-bp segment located upstream of the *TAS1R3* translation start site was indicated to be a part of a gene corresponding to human *MGC10334* or mouse *BC002216* (orthologue of human *MGC10334*) (http://www.ncbi.nlm.nih.gov/BLAST/) (see Fig. 3A), the sequence of the segment excluding the 346 bp was compared with the corresponding human and mouse sequences. The comparison indicated that the swine sequence from the translation start site to 317 bp upstream of the start site (designated as 317 bp sequence) showed a similarity to the corresponding human and mouse regions. The swine 317 bp sequence was then subjected to analysis of transcription factor binding sites (http://www.cbrc.jp/research/db/TFSEARCHJ.html), which revealed SRY and GATA-1/GATA-2 binding sites in the region (data not shown). The SRY binding site was also found in the corresponding human and mouse regions. When the swine sequence excluding the 317 bp and 346 bp sequences was subjected to the analysis of transcription factor binding sites using the above website, the analysis demonstrated 43 transcription factor binding sites, none of which, however, were commonly found in the corresponding human and mouse sequences (data not shown). These findings taken together indicated that the SRY binding site in the 317 bp sequence might function to control the transcription of *TAS1R3*.

Expression of TAS1R3 in swine tissues

The expression of *TAS1R3* in swine was investigated in tongue, heart, lung, stomach, intestine, liver, kidney, and testis by real-time PCR (Fig. 6), the results of which were normalized with reference to the amount of EGFP RNA added as a control along with the RNA samples. Tongue, kidney, and testis expressed the *TAS1R3* gene at a much higher rate than other tissues (Fig. 6). It was also demonstrated that heart, lung, and stomach expressed the gene significantly more than intestine and liver, though the extent of the elevations was small. The feature of *TAS1R3* gene expression in swine tissues examined was found to be essentially the same as that for mouse except that kidney expressed the gene as much as tongue in swine.

Determination of TAS1R3 gene expression sites in tissues

In order to investigate the localization of *TAS1R3* gene expression within various tissues, tongue, testis, and kidney were subjected to in situ hybridization using the RNA probes derived from exon 6. As shown in Fig. 7, tongue was found to express the gene in the circumvallate papillae (Fig. 7A), fungiform papillae (Fig. 7B), mucosal epithelium cells (Fig. 7A and 7B), lymphocytes in submucosal tissues of the lingual tonsil (Fig. 7C), and follicular B lymphocytes (Fig. 7D). Spermatogenic cells within the testis were also found to express the gene (Fig. 7E). Gene expression in kidney appeared uniform rather than specific to certain cells (data not shown). We have reached essentially the same in situ hybridization results using a different RNA probe from nt+137 to nt+317 (exon 1 and 2) (data not shown), providing supportive evidence for the findings obtained in the present study.

In order to confirm that swine B lymphocytes expressed *TAS1R3*, mature B lymphocytes were prepared from peripheral blood cells by a cell-sorter using an anti-CD21 antibody

Fig. 7. Expression of *TAS1R3* in swine tissues. Red and black arrows in **A** indicate tongue circumvallate papillae and mucosal epithelium, respectively; in **B**, they indicate tongue fungiform papillae and mucosal epithelium, respectively; (**C**) lymphocytes in submucosal tissue of lingual tonsil; (**D**) follicular B lymphocytes; and (**E**) spermatogenic cells in testis. (A1–E1) Results of in situ hybridization using RNA anti-sense probe (detection of *TAS1R3* sense message); (A2–E2) results of hybridization using RNA sense probe; and (A3–C3) staining with hematoxylin and eosin.

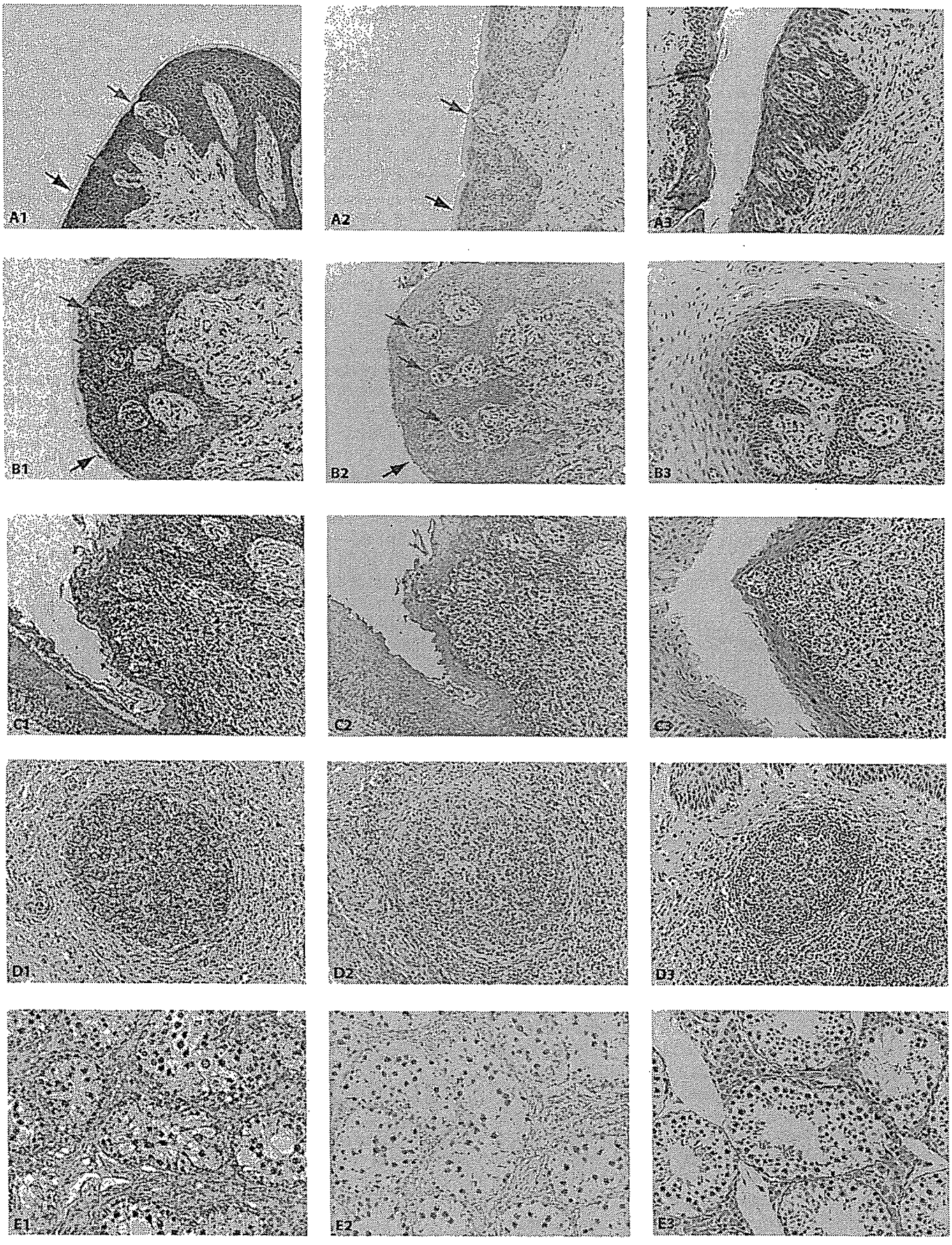
A1
A2
A3
B1
B2
B3
C1
C2
C3
D1
D2
D3
E1
E2
E3

to extract RNA from the lymphocytes. Real-time PCR using that RNA demonstrated the existence of a transcript from *TAS1R3* in B lymphocytes. However, since the amount of RNA prepared from the B lymphocytes was too small to be determined by UV absorbance, the amount of transcript in the B lymphocytes sample could not be directly compared with amounts of transcript in other samples (such as tongue). The DNA fragment amplified from B lymphocytes was cloned and sequenced, and found to be identical to that of *TAS1R3* cDNA. These findings confirmed the expression of *TAS1R3* in B lymphocytes, though the level of that expression could not be determined.

Exploitation of SNPs possibly related to tasting

The association between differences in sweet preference and sequence polymorphisms producing amino-acid substitutions has been previously reported in mouse (Max et al., 2001; Reed et al., 2004). Therefore, genomic DNAs from nine pigs of various breeds (see Materials and methods) were sequenced for the entire *TAS1R3* gene (position: 1055 to 6862 in the sequence with Accession No. AB162126), and the *TAS1R3* genomic sequences were compared. Eight SNPs in exons and five SNPs in introns were identified (described in the annotation of the sequence with Accession No. AB162126). However, no SNPs found in exons produced amino-acid substitutions (data not shown).

Discussion

TAS1R3 has been shown to be involved in sweet and umami tastes (along with TAS1R2 and TAS1R1) in mouse, and the sequence of the gene has been reported in mouse (Accession No. AL670236.9), rat (Accession No. NW_043877.1), gorilla (Accession No. AF545574), and human (Accession No. NT_077965.1). In the present study, the genomic structure of swine *TAS1R3* was determined, and *TAS1R3* expression was studied in various swine tissues. That gene was shown to reside on SSC6q22→q23, from which three distinct mRNA transcripts were generated: a 3,752-bp transcript derived from six exons was found in tongue, whereas in testis a 3,704-bp transcript from six exons, and a 3,630-bp transcript from seven exons were found. The 6-exons/5-introns structure was similar to those observed in human and mouse, but the 7-exons/6-introns structure of *TAS1R3* was first observed in swine. The expression pattern of the *TAS1R3* gene in tongue, testis, heart, lung, and liver was similar to that observed in mouse (Max et al., 2001). Additionally, a high expression with a level similar to that in testis was observed in kidney, a finding which had not previously been reported. In hybridization in situ, *TAS1R3* expression was detected in the tongue circumvallate papillae, fungiform papillae, mucosal epithelium, follicular B lymphocytes, lymphocytes in submucosal tissues of the lingual tonsil, and spermatogenic cells. In kidney, the expression appeared to be uniformly consistent rather than confined to specific cells. The expression of *TAS1R3* in B lymphocytes was further confirmed by real-time PCR using peripheral mature B lymphocytes, and by sequencing of the real-time PCR product.

Since the genomic structure, nucleotide sequence of cDNA, and amino-acid sequences of TAS1R3 are similar in swine, human and mouse, we hypothesized that functional transcription factor binding sites commonly exist in the three species. Based on this hypothesis, sequences upstream of the translation start site were compared to reveal an SRY binding site located 89 bp upstream of the translation start site as the one and only common site in the species. Hence, the SRY binding site is considered to serve as a functional binding site for the *TAS1R3* gene. However, in swine, two types of the exon/intron structures were involved in the generation of transcripts from *TAS1R3*, suggesting that another functional transcription factor binding site should exist. Genes such as the human collagen gene have previously been demonstrated to have functional transcription factor binding sites in their introns (Bornstein et al., 1987; Schultz et al., 1991). When the intron sequences of the three species were compared to identify common transcription factors, it was demonstrated that the Sp1 binding site was identified as a common site in swine and human intron 2. Therefore, it is possible that Sp1 would be another element in differential gene expression.

TAS1R3 expression was detected in the tongue circumvallate papillae, fungiform papillae, mucosal epithelium, follicular B lymphocytes, lymphocytes in submucosal tissues of the lingual tonsil, spermatogenic cells, kidney and peripheral mature B lymphocytes by both or either of real-time PCR and in situ hybridization. The expressions in circumvallate papillae and fungiform papillae were reported in mouse (Kitagawa et al., 2001; Max et al., 2001). However, expressions in tongue mucosal epithelium, kidney, and B lymphocytes have not been previously reported. In taste papillae, complexes of TAS1R1 and TAS1R3, and of TAS1R2 and TAS1R3 serve as the receptors for umami and sweet, respectively (Nelson et al., 2001, 2002). However, since no tasting function is considered to exist in tissues or cells other than the taste receptor cells, and since the types of cells expressing *TAS1R3* gene are different, it is possible that TAS1R3 is involved in different signal transductions in those cells via collaboration with proteins other than TAS1R1 and TAS1R2. In order to provide clues to infer the functions of *TAS1R3* in those cells, expressions of *TAS1R1* and *TAS1R2* should be examined specifically in those cells, while *TAS1R3* expression should be investigated throughout the differentiation processes of those cells.

Acknowledgements

The authors wish to thank Drs. Martine Yerle (INRA, France), Lawrence B. Schook (UIUC, USA), and Craig W. Beattie (UNR, USA) for supplying the IMpRH panel DNA. The authors also wish to thank Dr. Sue Galloway (AgResearch, New Zealand) for critical reading of our manuscript and suggestions in preparation of the manuscript.

References

Adler E, Hoon MA, Mueller KL, Chandrashekar J, Ryba NJ, Zuker CS: A novel family of mammalian taste receptors. Cell 100:693–702 (2000).

Awata T, Yamakuchi H, Kumagai M, Yasue H: Assignment of the tenascin gene *(HXB)* to swine chromosome 1q21.1→q21.3 by fluorescence in situ hybridization. Cytogenet Cell Genet 69: 33–34 (1995).

Bernhardt SJ, Naim M, Zehavi U, Lindemann B: Changes in IP3 and cytosolic Ca^{2+} in response to sugars and non-sugar sweeteners in transduction of sweet taste in the rat. J Physiol 490: 325–336 (1996).

Bornstein P, McKay J, Morishima JK, Devarayalu S, Gelinas RE: Regulatory elements in the first intron contribute to transcriptional control of the human alpha 1(I) collagen gene. Proc Natl Acad Sci USA 84:8869–8873 (1987).

Cummings TA, Daniels C, Kinnamon SC: Sweet taste transduction in hamster: sweeteners and cyclic nucleotides depolarize taste cells by reducing a K^+ current. J Neurophysiol 75:1256–1263 (1996).

Gilbertson TA, Avenet P, Kinnamon SC, Roper SD: Proton currents through amiloride-sensitive Na channels in hamster taste cells. Role in acid transduction. J Gen Physiol 100:803–824 (1992).

Gilbertson TA, Damak S, Margolskee RF: The molecular physiology of taste transduction. Curr Opin Neurobiol 10:519–527 (2000).

Kitagawa M, Kusakabe Y, Miura H, Ninomiya Y, Hino A: Molecular genetic identification of a candidate receptor gene for sweet taste. Biochem Biophys Res Commun 283:236–242 (2001).

Kiuchi S, Inage Y, Hiraiwa H, Uenishi H, Yasue H: Assignment of 280 swine genomic inserts including 31 microsatellites from BAC clones to the swine RH map (IMpRH map). Mamm Genome 13:80–88 (2002).

Kretz O, Barbry P, Bock R, Lindemann B: Differential expression of RNA and protein of the three pore-forming subunits of the amiloride-sensitive epithelial sodium channel in taste buds of the rat. J Histochem Cytochem 47:51–64 (1999).

Li X, Staszewski L, Xu H, Durick K, Zoller M, Adler E: Human receptors for sweet and umami taste. Proc Natl Acad Sci USA 99:4692–4696 (2002).

Lin W, Burks CA, Hansen DR, Kinnamon SC, Gilbertson TA: Taste receptor cells express pH-sensitive leak K^+ channels. J Neurophysiol 92: 2909–2919 (2004).

Lindemann B: Receptors and transduction in taste. Nature 413:219–225 (2001).

Max M, Shanker YG, Huang L, Rong M, Liu Z, Campagne F, Weinstein H, Damak S, Margolskee RF: *Tas1r3*, encoding a new candidate taste receptor, is allelic to the sweet responsiveness locus *Sac*. Nat Genet 28:58–63 (2001).

Mikawa S, Akita T, Hisamatsu N, Inage Y, Ito Y, Kobayashi E, Kusumoto H, Matsumoto T, et al: A linkage map of 243 DNA markers in an intercross of Gottingen miniature and Meishan pigs. Anim Genet 30:407–417 (1999).

Milan D, Hawken R, Cabau C, Leroux S, Genet C, Lahbib Y, Tosser G, Robic A, et al: IMpRH server: an RH mapping server available on the Web. Bioinformatics 16:558–559 (2000).

Nelson G, Hoon MA, Chandrashekar J, Zhang Y, Ryba NJ, Zuker CS: Mammalian sweet taste receptors. Cell 106:381–390 (2001).

Nelson G, Chandrashekar J, Hoon MA, Feng L, Zhao G, Ryba NJ, Zuker CS: An amino-acid taste receptor. Nature 416:199–202 (2002).

Ohtsuki T, Furuya S, Yamada T, Nomura S, Hata J, Yabe Y, Hosoda Y: Gene expression of noncollagenous bone matrix proteins in the limb joints and intervertebral disks of the *twy* mouse. Calcif Tissue Int 63:67–172 (1998).

Reed DR, Li S, Li X, Huang L, Tordoff MG, Starling-Roney R, Taniguchi K, West DB, et al: Polymorphisms in the taste receptor gene (*Tas1r3*) region are associated with saccharin preference in 30 mouse strains. J Neurosci 24:938–946 (2004).

Schultz JR, Tansey T, Gremke L, Storti RV: A muscle-specific intron enhancer required for rescue of indirect flight muscle and jump muscle function regulates *Drosophila* tropomyosin I gene expression. Mol Cell Biol 11:1901–1911 (1991).

Suzuki K, Asakawa S, Iida M, Shimanuki S, Fujishima N, Hiraiwa H, Murakami Y, Shimizu N, Yasue H: Construction and evaluation of a porcine bacterial artificial chromosome library. Anim Genet 31:8–12 (2000).

Suzuki Y, Sugano S: Construction of a full-length enriched and a 5′-end enriched cDNA library using the oligo-capping method. Methods Mol Biol 221:73–91 (2003).

Tumbelson ME, Schook LB: Advances in swine in biomedical research, in Tumbelson ME, Schook LB (eds): Advances in Swine in Biomedical Research, pp 1–4 (Plenum Press, New York 1996).

Yasue H, Ishibashi M: The oncogenicity of avian adenoviruses. III. In situ DNA hybridization of tumor line cells localized a large number of a virocellular sequence in few chromosomes. Virology 116:99–115 (1982).

Yerle M, Pinton P, Robic A, Alfonso A, Palvadeau Y, Delcros C, Hawken R, Alexander L, et al: Construction of a whole-genome radiation hybrid panel for high-resolution gene mapping in pigs. Cytogenet Cell Genet 82:182–188 (1998).

Zhao GQ, Zhang Y, Hoon MA, Chandrashekar J, Erlenbach I, Ryba NJ, Zuker CS: The receptors for mammalian sweet and umami taste. Cell 115:255–266 (2003).

Available online at www.sciencedirect.com
SCIENCE DIRECT
Leukemia Research 30 (2006) 1059–1062
Leukemia Research
www.elsevier.com/locate/leukres

Case report

Fulminant Epstein-Barr virus (EBV)-associated T-cell lymphoproliferative disorder with hemophagocytosis following autologous peripheral blood stem cell transplantation for relapsed angioimmunoblastic T-cell lymphoma

Norihiro Awaya[a,*], Akiko Adachi[a], Taisuke Mori[b], Hiroshi Kamata[a], Jin Nakahara[a], Kenji Yokoyama[a], Taketo Yamada[b], Masahiro Kizaki[a], Michiie Sakamoto[b], Yasuo Ikeda[a], Shin-ichiro Okamoto[a]

[a] *Division of Hematology, Department of Medicine, Keio University School of Medicine, Japan*
[b] *Department of Pathology, Keio University School of Medicine, Japan*

Received 23 September 2005; received in revised form 20 October 2005; accepted 23 October 2005
Available online 2 December 2005

Abstract

Post-transplant lymphoproliferative disorder (PTLD) is a complication that can develop after either solid-organ or hematopoietic stem cell transplantation (HSCT). T-cell PTLD is a rare disorder, especially following autologous HSCT. Here we report a case of T-cell PTLD which occurred after autologous peripheral blood stem cell transplantation (PBSCT) for relapsed angioimmunoblastic T-cell lymphoma (AILT). Three months after the transplant, the patient developed fever with elevated plasma Epstein-Barr virus (EBV)-PCR values. The patient subsequently developed pneumonitis, hepatomegaly and marked pancytopenia due to hemophagocytosis. The patient died of multi-organ failure, despite antiviral and steroid pulse therapy. Our post-mortem study confirmed the marked proliferation of EBV-infected T-cells that differed from the original AILT clone and macrophages/histiocytes were observed in the marrow, liver, lymph nodes and lungs. Phagocytosis was most evident in the bone marrow. The patient's AILT remained in complete remission. To the best of our knowledge, this is the first case of fulminant EBV-associated T-cell lymphoproliferative disorder (LPD) following autologous HSCT.

Keywords: Epstein-Barr virus; T-cell lymphoproliferative disorder; Hemophagocytosis; Autologous peripheral blood stem cell transplantation; Angioimmunoblastic T-cell lymphoma

1. Introduction

PTLD occurs as a consequence of immunosuppression in a solid-organ or hematopoietic allograft recipient. The overall incidence of PTLD following solid-organ transplant and standard T-cell repleted allogeneic bone marrow transplant is 1–3% [1] and has rarely been reported after autologous HSCT [2]. PTLD consists of a spectrum of disorders ranging from EBV-driven polyclonal proliferation resembling infectious mononucleosis to clonal EBV-positive B-cell lymphoma. In contrast to B-cell PTLD, T-cell PTLD is less frequent and is not usually associated with EBV [3]. Here, we report the case which developed clonal EBV-associated T-cell proliferation with hemophagocytosis following autologous PBSCT for relapsed AILT. This clinical presentation was compatible with previously reported fulminant T-cell LPD [4].

2. Case report

A 49-year-old Japanese male initially noticed lymphadenopathy in the right groin in December 2001, which

* Corresponding author at: 35 Shinanomachi, Shinjuku-ku, Tokyo 160-8582, Japan. Tel.: +81 3 5363 3785; fax: +81 3 3353 3515.
E-mail address: nawaya@sc.itc.keio.ac.jp (N. Awaya).

0145-2126/$ – see front matter © 2005 Elsevier Ltd. All rights reserved.
doi:10.1016/j.leukres.2005.10.022

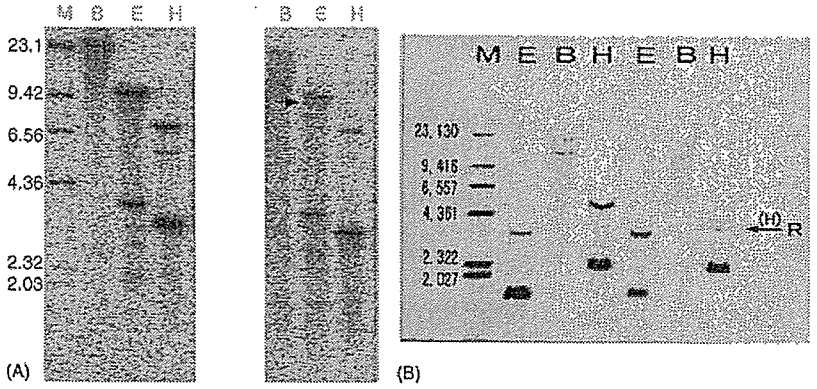

Fig. 1. Southern blot analysis for TCR gene rearrangement. (A) TCR β was positive when T-cell LPD developed after autologous HSCT. (B) In contrast, TCR γ was detected at the time of the initial diagnosis. The three left lanes serve as controls and the three right lanes represent patient samples in both experiments. M: molecular size marker (λDNA/Hind III), E: EcoR I, B: BamH I, H: Hind III.

spontaneously regressed without treatment. He later presented with recurring bilateral inguinal lymphadenopathy in November 2002 and the histological findings of a biopsy specimen from the right inguinal node were compatible with AILT. In situ hybridization for EBV-encoded small nuclear RNAs (EBER) and latent membrane protein (LMP) was positive and notably, EBER was detected in both the B- and T-cell populations. Complete remission was achieved after five cycles of CHOP (cyclophosphamide, doxorubicin, vincristine and prednisolone). Relapse was histologically confirmed when left cervical lymph node swelling developed in February 2004. Salvage chemotherapy (ESHAP; etoposide, cytarabine, cisplatin and methylprednisolone) was administered and 8.4×10^6/kg of G-CSF mobilized peripheral CD34-positive cells were collected from the patient and were cryopreserved. The patient was subsequently treated with MCVAC (ranimustine, cytarabine, etoposide and cyclophosphamide) and received autologous PBSCT in June 2004. The treatment course was only complicated with a low-grade fever for 2 weeks starting on day 27 post-transplant. The fever was

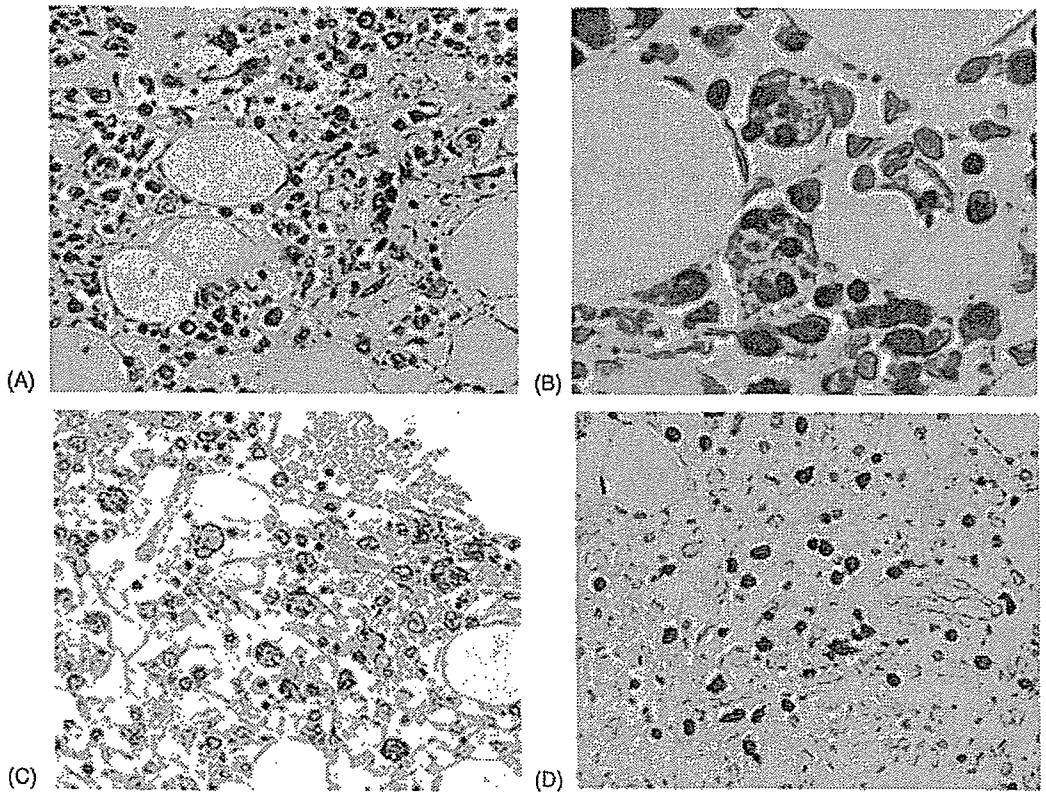

Fig. 2. Histological findings of the bone marrow at autopsy. (A) Hemophagocytosis was evident (hematoxylin and eosin, ×200). (B) High-power field (×1000). (C) Phagocytic cells were CD68-positive (×200). (D) EBER hybridization for CD3-positive cells (×200).

associated with a high EBV-PCR value of 10,000 copies/ml. The patient subsequently became afebrile and the EBV-PCR value decreased to 200 copies/ml without any antiviral treatment. In September 2004, he presented with fever and superficial lymphadenopathy. Laboratory data showed elevated values of lactate dehydrogenase (LDH), soluble interleukin-2 receptor (sIL-2R) and EBV-PCR (1000 copies/ml). Transient amelioration of fever and lymphadenopathy occurred after the administration of valaciclovir. Nevertheless, interstitial pneumonitis developed in October, in addition to the abovementioned abnormalities and the patient was admitted to our hospital in November. On admission, physical examination revealed a temperature of 38.3 °C, fine crackles to auscultation of the lungs, superficial lymphadenopathy of up to 1 cm in diameter and hepatomegaly palpated 2 cm below the right costal margin. Laboratory values on admission were as follows: white blood cells 2600/μl, hemoglobin 10.5 g/dl, platelet count 4.9×10^4/μl, LDH 522 IU/l, sIL-2R 4330 U/ml, IgG 918 mg/dl and EBV-PCR 9000 copies/ml. The patient was again placed on valaciclovir; however, the fever and lymphadenopathy persisted, with the subsequent development of pancytopenia, which required both packed red cell as well as platelet transfusion. Serum ferritin and triglyceride levels were also elevated. Treatment with foscarnet and high-dose steroids was ineffective and the patient died of multi-organ failure. The LDH, sIL-2R and EBV-PCR values just prior to the patient's death were 10,140 IU/l, 32,300 U/ml and 20,000 copies/ml, respectively. Permission for autopsy was granted. Autopsy revealed the presence of CD3-positive cells in the marrow, portal area of the liver, lymph nodes and lungs and those cells were also positive for EBER, as determined by serial sections. DNA rearrangement of T-cell receptor (TCR) β was positive (Fig. 1A); however, no DNA rearrangement for TCR γ was detected, although tests for this rearrangement had originally been positive at the time of the initial diagnosis of AILT (Fig. 1B). CD3-positive cells did not express CD4 (data not shown), which was positive for the original AILT cells. These findings suggested that these EBV-infected T-cells were derived from T-cell clones that differed from the original AILT clone and that the patient's AILT had remained in remission. Another significant finding of this case was the presence of hypocellularity in the marrow, which was associated with the proliferation of CD68-positive macrophages and marked hemophagocytosis (Fig. 2A–C). CD68-positive macrophages were also noticeable in the liver, lymph nodes and lungs. Again, EBER was positive for T-cells in the marrow (Fig. 2D).

3. Discussion

PTLD represents a spectrum of EBV-related clinical diseases, from a polyclonal mononucleosis-like illness to a monomorphic disease with sufficient cytologic and architectural atypia to be diagnosed as a lymphoma. In patients who undergo solid-organ transplantation, high-levels of immunosuppression are considered as a risk factor and the incidence of PTLD has been reported to approach 10% in lung transplant patients, where high-levels of immunosuppression are required [5]. Generally, the risk of PTLD is between 1 and 3% in recipients of organ transplant or T-cell repleted allogeneic HSCT [1,5]. In contrast, only a few cases have been described of EBV-associated PTLD following autologous HSCT [6–8]. Yufu et al. reported the first case of EBV-associated T-cell PTLD following autologous PBSCT for relapsed Hodgkin's disease [2]. In contrast to the present case, the patient described in their report presented with clonal CD8-positive cell proliferation and had a clinical course similar to that of chronic active EBV infection. The clinical features of our case were more similar to those of patients with fulminant T-cell LPD described by Quintanilla-Martinez et al. [4]. The latter cases were characterized by fever, liver failure, pancytopenia secondary to hemophagocytosis, hepatosplenomegaly and many showed no significant lymphadenopathy. The clinical course was literally fulminant and most of the patients died within days to months [4]. Also in their cases, EBV infected T-cell clones were detected in the liver, spleen, or lymph nodes. Our post-mortem study also clearly demonstrated a correlation with EBV positivity, as determined by EBER hybridization, with CD3 staining.

EBV is capable of infecting not only B-cells, but also T-cells and natural killer (NK) cells and it is known to cause LPD or lymphoma [4,9,10]; however, most PTLDs are of B-cell origin and are associated with EBV infection. Approximately 4–14% of adult PTLDs are of T-cell origin, which is rarely associated with EBV infection and to date, only 14 cases have been reported [1,11,12]. Interestingly, a phenotype switch between the B- and T-cell types has been described in a single case with immunodeficiency [13]. Our case showed the coexistence of infected B- and T-cell populations at the initial presentation of the disease, which appears to be a characteristic of AILT [14]. AILT itself is known to be susceptible for the development of B-LPD [15]; however, the factors responsible for influencing the lineage commitment of LPD remain undetermined at present. In the present patient, no recurrence of AILT was observed, as based on the lack of CD4 expression, as well as on the absence of TCR γ rearrangement, both of which had originally been present at the time of the patient's initial diagnosis of AILT. As regards T-cell PTLD with hemophagocytosis, only a single post-liver transplantation pediatric case has been reported to date [16]. To the best of our knowledge, this is the first case reported in the literature of fulminant T-cell PTLD with hemophagocytosis following autologous HSCT.

One of the treatment options for PTLD following solid-organ transplantation or allogeneic HSCT would be the withdrawal of immunosuppressive therapy. However, such an approach would not be applicable for PTLD after autologous HSCT. Antiviral thymidine kinase inhibitors, ganciclovir and acyclovir, are theoretically ineffective against EBV in vivo, because EBV survives as an episome outside of the lymphocytic genome. It was of note that a transient effect of

valaciclovir was observed in the present case; moreover, a similar clinical course was previously obtained with valaciclovir treatment [17]. Further investigation in a combination of EBV-PCR monitoring and the preemptive use of valaciclovir might be warranted in cases of AILT after autologous HSCT.

Acknowledgments

The authors would like to thank the nurses in the ward, Dr. Mariko Yabe, Dr. Yuiko Tsukada, Dr. Takayuki Shimizu, Dr. Toyotaka Iguchi, Dr. Chien-Kang Chen, Dr. Akihiro Yokoyama and Dr. Takehiko Mori for their excellent care to the patient.

Contributions. N. Awaya provided drafting of the manuscript and important intellectual content. A. Adachi, H. Kamata and J. Nakahara collected and organized the data. T. Mori, T. Yamada and M. Sakamoto examined and provided pathological materials. T. Mori was responsible for autopsy reports. K. Yokoyama, M. Kizaki and Y. Ikeda provided critical revisions. S. Okamoto provided critical revisions and gave final approval.

References

[1] Lundell R, Elenitoba-Johnson KS, Lim MS. T-cell post-transplant lymphoproliferative disorder occurring in a pediatric solid-organ transplant patient. Am J Surg Pathol 2004;28:967–73.

[2] Yufu Y, Kimura M, Kawano R, Noguchi Y, Takatsuki H, Uike N, et al. Epstein-Barr virus-associated T-cell lymphoproliferative disorder following autologous blood stem cell transplantation for relapsed Hodgkin's disease. Bone Marrow Transpl 2000;26:1339–41.

[3] Bhatia S, Ramsay NK, Steinbuch M, Dusenbery KE, Shapiro RS, Weisdorf DJ, et al. Malignant neoplasms following bone marrow transplantation. Blood 1996;87:3633–9.

[4] Quintanilla-Martinez L, Kumar S, Fend F, Reyes E, Teruya-Feldstein J, Kingma DW, et al. Fulminant EBV(+) T-cell lymphoproliferative disorder following acute/chronic EBV infection: a distinct clinicopathologic syndrome. Blood 2000;96:443–51.

[5] Loren AW, Porter DL, Stadtmauer EA, Tsai DE. Post-transplant lymphoproliferative disorder: a review. Bone Marrow Transpl 2003;31: 145–55.

[6] Shepherd JD, Gascoyne RD, Barnett MJ, Coghlan JD, Phillips GL. Polyclonal Epstein-Barr virus-associated lymphoproliferative disorder following autografting for chronic myeloid leukemia. Bone Marrow Transpl 1995;15:639–41.

[7] Hauke RJ, Greiner TC, Smir BN, Vose JM, Tarantolo SR, Bashir RM, et al. Epstein-Barr virus-associated lymphoproliferative disorder after autologous bone marrow transplantation: report of two cases. Bone Marrow Transpl 1998;21:1271–4.

[8] Lones MA, Kirov I, Said JW, Shintaku IP, Neudorf S. Post-transplant lymphoproliferative disorder after autologous peripheral stem cell transplantation in a pediatric patient. Bone Marrow Transpl 2000;26:1021–4.

[9] Kawa K. Epstein-Barr virus-associated diseases in humans. Int J Hematol 2000;71:108–17.

[10] Kasahara Y, Yachie A, Takei K, Kanegane C, Okada K, Ohta K, et al. Differential cellular targets of Epstein-Barr virus (EBV) infection between acute EBV-associated hemophagocytic lymphohistiocytosis and chronic active EBV infection. Blood 2001;98:1882–8.

[11] Leblond V, Davi F, Charlotte F, Dorent R, Bitker MO, Sutton L, et al. Post-transplant lymphoproliferative disorders not associated with Epstein-Barr virus: a distinct entity? J Clin Oncol 1998;16: 2052–9.

[12] Nelson BP, Nalesnik MA, Bahler DW, Locker J, Fung JJ, Swerdlow SH. Epstein-Barr virus-negative post-transplant lymphoproliferative disorders: a distinct entity? Am J Surg Pathol 2000;24:375–85.

[13] Imashuku S, Miyagawa A, Chiyonobu T, Ishida H, Yoshihara T, Teramura T, et al. Epstein-Barr virus-associated T-lymphoproliferative disease with hemophagocytic syndrome, followed by fatal intestinal B-lymphoma in a young adult female with WHIM syndrome. Warts, hypogammaglobulinemia, infections and myelokathexis. Ann Hematol 2002;81:470–3.

[14] Anagnostopoulos I, Hummel M, Finn T, Tiemann M, Korbjuhn P, Dimmler C, et al. Heterogeneous Epstein-Barr virus infection patterns in peripheral T-cell lymphoma of angioimmunoblastic lymphadenopathy type. Blood 1992;80:1804–12.

[15] Zettl A, Lee SS, Rudiger T, Starostik P, Marino M, Kirchner T, et al. Epstein-Barr virus-associated B-cell lymphoproliferative disorders in angioimmunoblastic T-cell lymphoma and peripheral T-cell lymphoma, unspecified. Am J Clin Pathol 2002;117:368–79.

[16] George TI, Jeng M, Berquist W, Cherry AM, Link MP, Arber DA. Epstein-Barr virus-associated peripheral T-cell lymphoma and hemophagocytic syndrome arising after liver transplantation: case report and review of the literature. Pediatr Blood Cancer 2005;44:270–6.

[17] Battegay M, Berger C, Rochlitz C, Hurwitz N, Hirsch HH, De Geyter C, et al. Epstein-Barr virus load correlating with clinical manifestation and treatment response in a patient with angioimmunoblastic T-cell lymphoma. Antivir Ther 2004;9:453–9.

基礎研究成果の臨床応用推進研究事業

ヒト化CD26抗体の難治性免疫疾患
（クローン病、GVHDなど）への治療法開発

平成18年度　総括・分担研究報告書

平成19年4月10日発行

発行：主任研究者　森本　幾夫
〒108-8639　東京都港区白金台4-6-1
東京大学医科学研究所　先端医療研究センター　免疫病態分野
TEL：03-5449-5546